

# Analysis of Filtered Thermal-Fluid Video Data From Downward Facing Boiling Experiments

recorded from a pool boiling apparatus for physics-based understanding of the associated phenomena. [DOI: 10.1115/1.4039470]

Keywords: nuclear plant safety, video data, filtering

## Chi-Shih Jao

Department of Electrical Engineering,  
Pennsylvania State University,  
University Park, PA 16802  
e-mail: cxj36@psu.edu

## Faith R. Beck

Department of Mechanical and Nuclear Engineering,  
Pennsylvania State University,  
University Park, PA 16802  
e-mail: frb115@psu.edu

## Nurali Virani

General Electric Global Research Center,  
Niskayuna, NY 12309  
e-mail: nurali.virani88@gmail.com

## Fan-Bill Cheung

Fellow ASME  
Department of Mechanical and  
Nuclear Engineering,  
Pennsylvania State University,  
University Park, PA 16802  
e-mail: fxc46@psu.edu

## Asok Ray<sup>1</sup>

Fellow ASME  
Department of Mechanical and  
Nuclear Engineering,  
Pennsylvania State University,  
University Park, PA 16802  
e-mail: axr2@psu.edu

*During severe accidents in a nuclear power plant, in-vessel cooling may be required to mitigate the risk of vessel failure in the event of core meltdown and subsequent corium contamination. This cooling technique, known as in-vessel retention (IVR), entails flooding the reactor cavity with water. If the temperatures are sufficiently high, IVR may cause downward facing boiling (DFB) on the outer surface of the reactor pressure vessel (RPV), which gives rise to two-phase thermal-hydraulic phenomena. The regimes in DFB may range from film boiling to nucleate boiling, where the efficiency of cooling varies immensely between these two. In the DFB geometry under consideration (i.e., a hemispherical vessel), the collected signals/images are heavily contaminated by unavoidable noise and spurious disturbances, which hinder the extraction of pertinent information, such as film thickness and the boiling cycle. This paper proposes a wavelet-based filtering of sensor measurements for denoising of the nonstationary signals with the future objective of estimating the thickness of vapor films in real time, as needed for process monitoring and control. The proposed concept has been validated with experimental data*

<sup>1</sup>Corresponding author.

Contributed by the Dynamic Systems Division of ASME for publication in the JOURNAL OF DYNAMIC SYSTEMS, MEASUREMENT, AND CONTROL. Manuscript received October 5, 2017; final manuscript received February 16, 2018; published online March 27, 2018. Assoc. Editor: Sergey Nersisov.

## 1 Introduction

Nuclear power plants are a source of safe and consistent energy under well-controlled operating conditions. Nevertheless, radiation protection is one of the biggest concerns in the design and maintenance of nuclear power plants. This is realized through multiple layers of protection (e.g., holding of fission gases by the fuel pellets themselves and cladding around the fuel rods) for safekeeping of the radioactive materials. All of these layers are housed inside the reactor pressure vessel (RPV), which is retained inside a containment building. During a severe accident, fuel pellets rupture and the fuel rod cladding melts, which can cause the meltdown of the reactor core, with molten corium relocating downward into the bottom head of the RPV. In order to contain the radioactive molten corium within the reactor, the reactor cavity is flooded with coolant to submerge the entire RPV. This method, also known as in-vessel retention (IVR) through external reactor vessel cooling allows removal of the decay heat from the molten corium through the vessel wall by downward facing boiling (DFB) on the outer surface of the vessel. During such accidents, it is crucial to maintain the integrity of the lower head of the RPV to achieve IVR, thus mitigating the risk of containment failure [1–3].

Efficient heat transfer during DFB on the RPV in an accident scenario is of critical importance, because the structural integrity of the vessel depends on the ability to transfer heat to the coolant. While there are different boiling regimes associated with downward facing surfaces, the two most significant are film and nucleate boiling. In film boiling, the heat transfer coefficient is much smaller than that in nucleate boiling. As such, the vapor film acts as an insulating surface from which heat transfer cannot take place efficiently [4,5]. When the film is broken under nucleate boiling after achieving the critical heat flux, thermal energy can be dissipated much faster since liquid is able to make direct contact with the heated surface. The regime change from film to nucleate boiling is of much importance because, if left too long under film boiling, the structural integrity of RPV may be compromised, resulting in possible corium contamination.

A scaled version of the RPV- quenching experiment has been performed on the subscale boundary layer boiling facility at Pennsylvania State University, as seen in Fig. 1(a). At this facility, the act of drowning the downward-facing hemisphere in a pool of water causes low-frequency vibration as the vessel rocks back and forth atop a support structure, which is positioned above the cylindrical vessel. This rocking motion of the vessel contaminates the acquired signals and the resulting low frequency vibration is referred to as the “inherent artifact” (IA) signal in the remainder of this paper. This externally imposed signal is not part of the actual, physical process induced by DFB, and so it must be removed. The original one-dimensional two-phase vapor film signals, extracted from the high-speed video images, are corrupted by the IA signal, as discussed in detail in Sec. 2. Therefore, noise filtering is essential for accurately extracting the signal. The data collected from these experiments have been analyzed to understand the physics involved in such nontraditional flow geometries.

For signal conditioning that includes denoising, the acquired raw data are decomposed into three parts: (1) the vapor film signal, (2) the IA signal, and (3) any additive noise. A common property of the vapor film and IA signals is that they are both nonstationary; therefore, a Fourier transform (FT) or a windowed Fourier transform (WFT) may not be appropriate for analyzing these signals. This is so because FT merely generates average frequency information, instead of time-dependent local frequency characteristics, and WFT uses a fixed short-length window to find the local frequency of a signal. For a WFT, the window size may

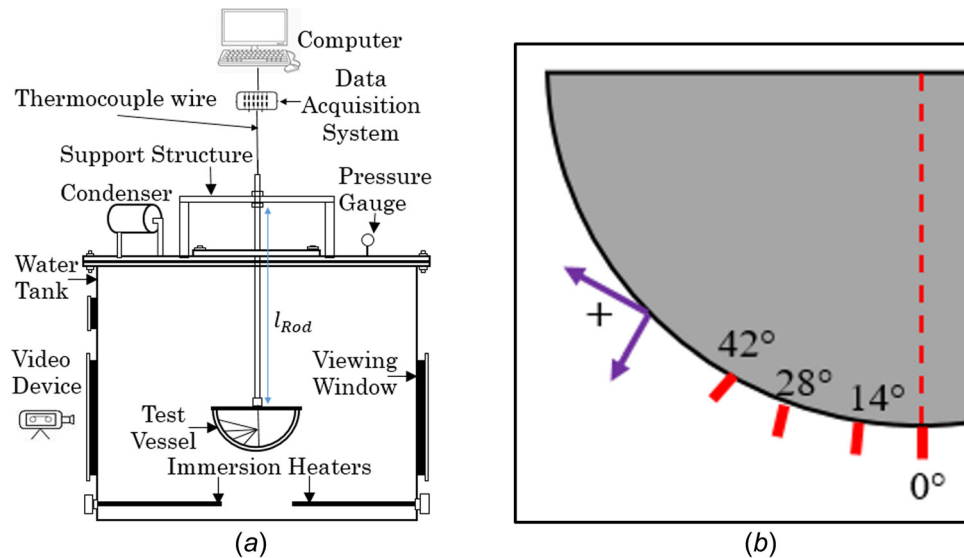


**Fig. 1 The pool boiling apparatus: (a) schematic diagram of the experimental apparatus and (b) measurement angles  $\phi$**

not be flexible, and therefore WFT also has not been used to analyze the vapor film and IA signals. Unlike FT and WFT, wavelet analysis transforms a signal from the time domain to a scaled domain with a scalable mother wavelet [6], permitting the signal to be decomposed into localized oscillating components. Hence, wavelet analysis is an ideal tool for analyzing the nonstationary two-phase vapor-film signals. In general, wavelet transforms have been widely used in the field of signal denoising because every empirical wavelet coefficient contributes noise of variance, but only very few wavelet coefficients contribute to the actual signal.

Recently, researchers have started to apply wavelet analysis in the field of two-phase flow. For example, De Kerpel et al. [7] used wavelet variance values to generate feature spaces for two-phase flow regimes in a horizontal tube. Additionally, Euh et al. [8] used wavelet analysis for two-phase flow pattern identification by determining the void fraction from a multichannel impedance void meter in vertical-upward air–water flow. To the best of our knowledge, no one has used wavelet analysis for the purpose of filtering two-phase, thermal-hydraulic signals. From these perspectives, the major contributions of this paper are as follows:

- (1) identification of a critical parameter (i.e., the IA frequency) that largely determines the thermal-hydraulic dynamics during pool boiling;
- (2) wavelet-based denoising of two-phase thermal-fluid signals generated by DFB; and
- (3) experimental validation of the above items on a laboratory-scale apparatus.

This paper is organized into the following sections: Section 2 addresses acquisition and preprocessing of experimental data; Sec. 3 discusses the experimental results; Sec. 4 summarizes and concludes the paper with recommendations for future research.

## 2 Data Acquisition and Preprocessing

This section addresses the preprocessing of high-speed video data acquired from an experimental apparatus to capture the underlying physics of pool boiling.

**2.1 Description of the Experimental Apparatus.** In the experimental part of this work, a downward-facing hemisphere has been heated and quenched in water and high-speed images are recorded at 650 frames per second (fps) and are processed to determine vapor formation. The vapor edge is then detected and

used to estimate the thickness of the time-dependent vapor film through the quenching process. The objective of this experiment is to provide physical insight into the dynamic process of vapor film formation and its transition to nucleate boiling.

Figure 1(a) presents a schematic view of the pool boiling apparatus, which consists of a cylindrical water tank (1.14 m tall and 1.2 m wide), support structure, and video and data acquisition systems. This configuration simulates the reactor cavity of a nuclear power plant, which is sufficiently large to reduce recirculation motions generated due to boiling. The vessel is made of 304-grade stainless steel, having an outside diameter of  $\sim 30$  cm, a wall thickness of  $\sim 2.5$  mm. Additionally, there are two large viewing windows of diameter  $\sim 0.558$  m are installed on either side of the tank to visualize the boiling process on the outer surface of the vessel. Four 36-gauge K-type thermocouples are spot welded along an arc starting from bottom center up to the equator of the vessel at 0 deg, 14 deg, 28 deg, and 42 deg, as seen in Fig. 1(b). In order to negate the radial variation of temperature in the vessel,  $\sim 3.8$  mm diameter holes with a depth of  $\sim 1.9$  mm are drilled along prescribed angular locations. The thermocouples are spot-welded as close as possible to the center of the drilled holes. Prior to quenching, the vessel is heated to  $400^\circ\text{C}$  (well above the minimum film boiling temperature of  $275^\circ\text{C}$ ), and the bath temperature is raised to the level of prescribed subcooling before the heated vessel is plunged vertically into the tank.

**2.2 Edge Detection.** In the pool boiling experiment, the vessel undergoes nonstationary, low-frequency, man-made vibrations that are generated by physically plunging the vessel into the tank. This section discusses how these IA vibrations affect the signals to be analyzed.

High-speed video recordings have been used to capture the instantaneous film thickness at 650 fps. In order to measure the film thickness using the high-speed video data, the edge of the film needs to be detected. The first step is to use color thresholding, which converts a colored image to a binary image. Then, using edge detection, the binary edge information is extracted using a Laplacian of Gaussian filter [9]. Figure 2(a) shows an example of the raw image (left) and the resulting detected edge (right). Once the edge information is extracted, a polar-to-Cartesian coordinate transformation is used to obtain the film thickness at each angular location, at any instant in time [10]. The location of the center and radius of the vessel (obtained from

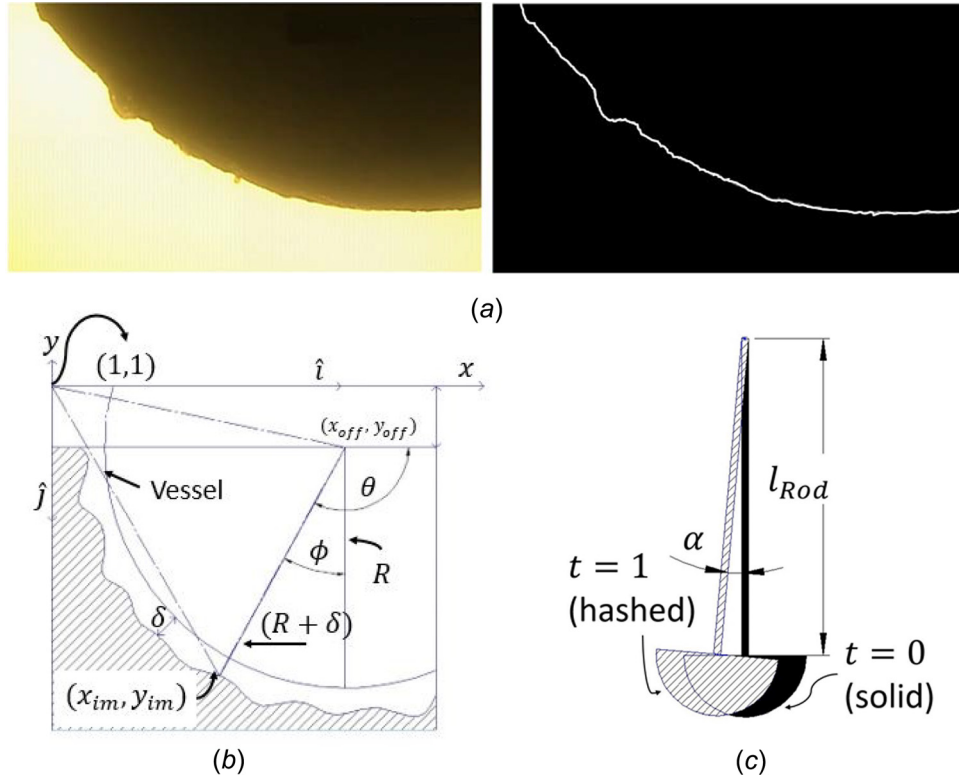


**Fig. 2 (a) Raw and detected edge images, (b) geometry of the vessel for vapor film extraction, and (c) schematic of IA vibration**

a vessel without any film) are used for the coordinate transformations.

**2.3 Conversion of Two-Dimensional Image to One-Dimensional Signal.** After the vapor film edge is detected, the film thickness is extracted from the image sequence. The resulting data are converted from cylindrical to Cartesian coordinates to compute the distance between the vapor film edge and the surface of the vessel at a particular angle; this distance is referred to as the *vapor film thickness*. For the analysis, the vessel is assumed to remain fixed at one particular location, and hence, the effects of IA are not yet removed. To precisely calculate the vapor film thickness at a given angle, several geometric parameters are introduced, as listed in the Nomenclature section.

The radius  $R$  and the offset parameters,  $x_{off}$  and  $y_{off}$ , are measured from a circle that is fit to a vessel image, devoid of vapor bubbles or film. The measurement angle  $\phi$ , having values of 0 deg, 14 deg, 28 deg, and 42 deg, represents the desired angle of film thickness extraction. The position  $(x_{im}, y_{im})$  is directly taken from the extracted vapor film edge. The parameter  $\theta$  is used for convenience to calculate the measurement angle  $\phi$  and has a 90 deg angle difference with  $\phi$  (i.e.,  $\phi = \theta - 90$  deg). The parameters  $\theta$  and  $\delta$  are derived from Fig. 2(b) as described below. The expression for  $(R + \delta)$  is

$$(R + \delta) = (R + \delta)\cos(\theta)\hat{i} + (R + \delta)\sin(\theta)\hat{j} \quad (1)$$

The vector starting from origin (1, 1) to the center of the vessel  $(x_{off}, y_{off})$  is

$$(x_{off} - 1)\hat{i} - (y_{off} - 1)\hat{j} \quad (2)$$

and the vector from origin to  $(x_{im}, y_{im})$  is

$$(x_{im} - 1)\hat{i} - (y_{im} - 1)\hat{j} \quad (3)$$

By vector addition, as shown in Fig. 2(b), the summation of Eqs. (2) and (3) yields

$$\begin{aligned} & [(R + \delta)\cos(\theta)\hat{i} + (R + \delta)\sin(\theta)\hat{j}] + [(x_{off} - 1)\hat{i} - (y_{off} - 1)\hat{j}] \\ & = (x_{im} - 1)\hat{i} - (y_{im} - 1)\hat{j} \end{aligned} \quad (4)$$

where Eq. (4) is decomposed into the  $\hat{i}$  and  $\hat{j}$  directions as

$$\hat{i}: (R + \delta)\cos(\theta) + (x_{off} - 1) = (x_{im} - 1) \quad (5)$$

$$\hat{j}: (R + \delta)\sin(\theta) + (y_{off} - 1) = -(y_{im} - 1) \quad (6)$$

A closed form of  $\delta$  is obtained from Eqs. (5) and (6) as

$$((R + \delta)\cos(\theta))^2 + ((R + \delta)\sin(\theta))^2 = (x_{im} - x_{off})^2 + (y_{im} - y_{off})^2 \quad (7)$$

$$\delta = \sqrt{(x_{im} - x_{off})^2 + (y_{im} - y_{off})^2} - R \quad (8)$$

It is noted that, in the above equations,  $x_{im}$  and  $y_{im}$  may vary with time, while the other geometric parameters remain constant; therefore, the parameter  $\delta$  is expressed as  $\delta(t)$ .

An expression for  $\theta$  is obtained by using the information from both  $\hat{i}$  and  $\hat{j}$  coordinates

$$\sin(\theta) = \frac{-y_{im} + y_{off}}{(R + \delta)} \text{ and } \cos(\theta) = \frac{x_{im} - x_{off}}{(R + \delta)} \quad (9)$$

$$\frac{\sin(\theta)}{\cos(\theta)} = \frac{-y_{im} + y_{off}}{x_{im} - x_{off}} \quad (10)$$

A closed-form expression for  $\theta$  is as follows:

$$\theta = \tan^{-1} \frac{-y_{im} + y_{off}}{x_{im} - x_{off}} \quad (11)$$

Here,  $\theta$  is treated as a constant while extracting the signal at a particular angle. In order to precisely determine  $\delta$ , the parameter  $\theta$  is first calculated with respect to different values of  $x_{im}$  and  $y_{im}$ .

Next, a point  $(x_{im}, y_{im})$  is chosen on the detected edge in Fig. 2(b) such that Eq. (11) yields the desired  $\theta$  based on the measurement angle  $\phi$ . For example, to extract the signal at  $\phi = 14$  deg, the desired  $\theta$  is set to be  $14 \text{ deg} + 90 \text{ deg} = 104 \text{ deg}$ . Then, the chosen pair  $(x_{im}, y_{im})$  is used in Eq. (8) to calculate  $\delta$ .

**2.4 Construction of the Inherent Artifact Signal.** It appears from the recorded video data that the IA vibrations behave as pendulum-like oscillations, as displayed in Fig. 2(c). Therefore, the IA frequency would have a larger impact on the signals than those that are extracted at higher angles  $\alpha$ . The IA vibrations significantly affect  $x_{off}$  and  $y_{off}$ , such that it is incorrect to assume that they are constants; hence, the values of  $x_{off}$  and  $y_{off}$  must vary with time in the presence of IA signals. These variations directly affect the computation of  $\theta$  and  $\delta$ . Contamination of  $\delta$  can be removed, in spite of the altered signal amplitude, by using signal processing tools (see Fig. 2(c)).

**2.5 Wavelet Analysis of Thermal-Fluid Signals.** The collected two-phase signal  $f$  is decomposed into three components as

$$f = f_{IA} + f_B + f_N \quad (12)$$

where  $f_{IA}$  is the (nonstationary) IA signal,  $f_B$  is the (nonstationary) vapor film signal, and  $f_N$  is the additive noise.

This paper uses multiresolution analysis (MRA) [6] to denoise the two-phase signal in the following steps:

- (1) choice of an appropriate mother wavelet;
- (2) decomposition of the signal into different scale levels;
- (3) detection of wavelet coefficients from the scale levels that have higher signal-to-noise-ratios; and
- (4) reconstruction of the desired “denoised” signal from the selected wavelet coefficients.

### 3 Experimental Results and Discussion

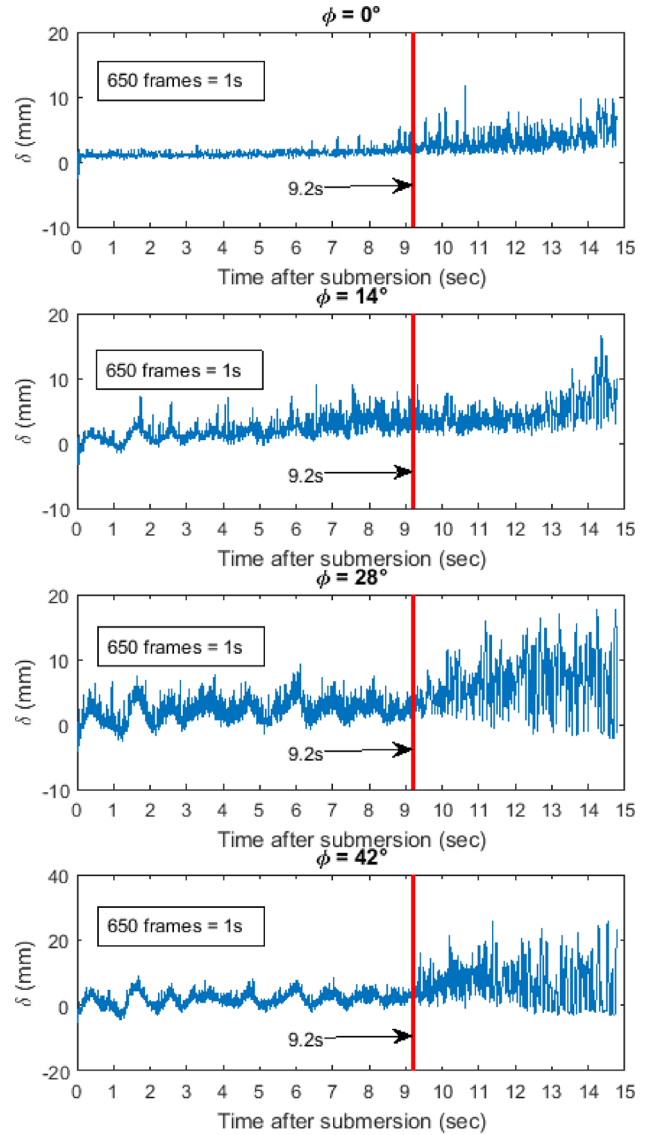
This section presents and discusses the results of analysis. While edge detection and signal extraction are described in Secs. 2.1 and 2.2, respectively, the following paragraphs describe the two-phase signals and their analyses.

Figure 3 displays typical profiles of two-phase thermal-hydraulic signals at  $\phi = 0$  deg, 14 deg, 28 deg, and 42 deg, respectively, for the liquid bath temperature of  $97^\circ\text{C}$ . These signals are extracted with constant values,  $x_{off}$  and  $y_{off}$ , of the offset coordinate positions. The data sets in Fig. 3 include the IA signal and an unknown additive noise. Two important observations from these signals are discussed below.

First, from each plot in Fig. 3, the behavior of the signals before and after  $\sim 9.2$  s is quite different. The rationale is that, in the first  $\sim 9.2$  s, the temperature of the vessel is still well above the minimum film boiling temperature. As the temperature of the vessel wall decreases (due to quenching), the vapor film is in the process of transitioning from film to nucleate boiling. This transition causes a rise in the local film thickness, which is attributed to the quench progression on the downward facing hemisphere.

Second, it is observed that in the first  $\sim 9.2$  s there is a low-frequency signal, the amplitude of which changes with the angular position  $\phi$ . This low-frequency signal is most clearly observable at  $\phi = 42$  deg and is barely detectable at  $\phi = 0$  deg. Since the IA signal results in pendulum-like oscillations, it would have a larger impact on the signals at higher angles, which leads to the conclusion that the low-frequency disturbances are caused primarily by this phenomenon. In fact, the IA frequency exists throughout the entire signal, but the vapor film becomes thicker at the critical time of  $\sim 9.2$  s, and so the effects of this vibration are less noticeable in the signal at later times.

**3.1 Identification of the Inherent Artifact Signal.** Due to the nature of the IA frequency and the geometry of the vessel, the



**Fig. 3 Profiles of vapor film thickness estimation at  $97^\circ\text{C}$  bath temperature. The thick vertical lines indicate the time epoch (i.e., 9.2 s) at which the signal behavior changes significantly.**

effects of this vibration are more noticeable at higher angles. Therefore, wavelet coefficients are chosen so that they decrease in intensity proportional to the angular location. It is seen in Fig. 3 that the IA signals are most dominant in the first  $\sim 9.2$  s of the collected signal at  $\phi = 42$  deg. Then, the MRA with a wavelet basis of db45 is used to analyze the first  $\sim 9.2$  s ( $\sim 6000$  frames) of the collected signals. The results are shown in Fig. 4, where the scales are dyadic, i.e., a sequence in powers of 2.

In Fig. 4, the wavelet coefficients corresponding to scales of 256 and 512 have larger intensities than other scales. The intensities of these two scales monotonically decrease at lower angles of  $\phi = 28$  deg, 14 deg, and 0 deg in Fig. 4. It is concluded that the coefficients of the db45 wavelet corresponding to the scales of 256 and 512 directly correlate with the IA signal.

The extracted IA signal has units of mm, but the IA vibration is a pendulum-like oscillation. To find out how the IA vibration generates an angle  $\alpha$ , an adaptive method is used as follows:

- (1) Choice of an initial negative value for  $\beta$ .
- (2) Dynamical modeling of the offset coordinates  $x_{off}$  and  $y_{off}$  with respect to the IA signal as

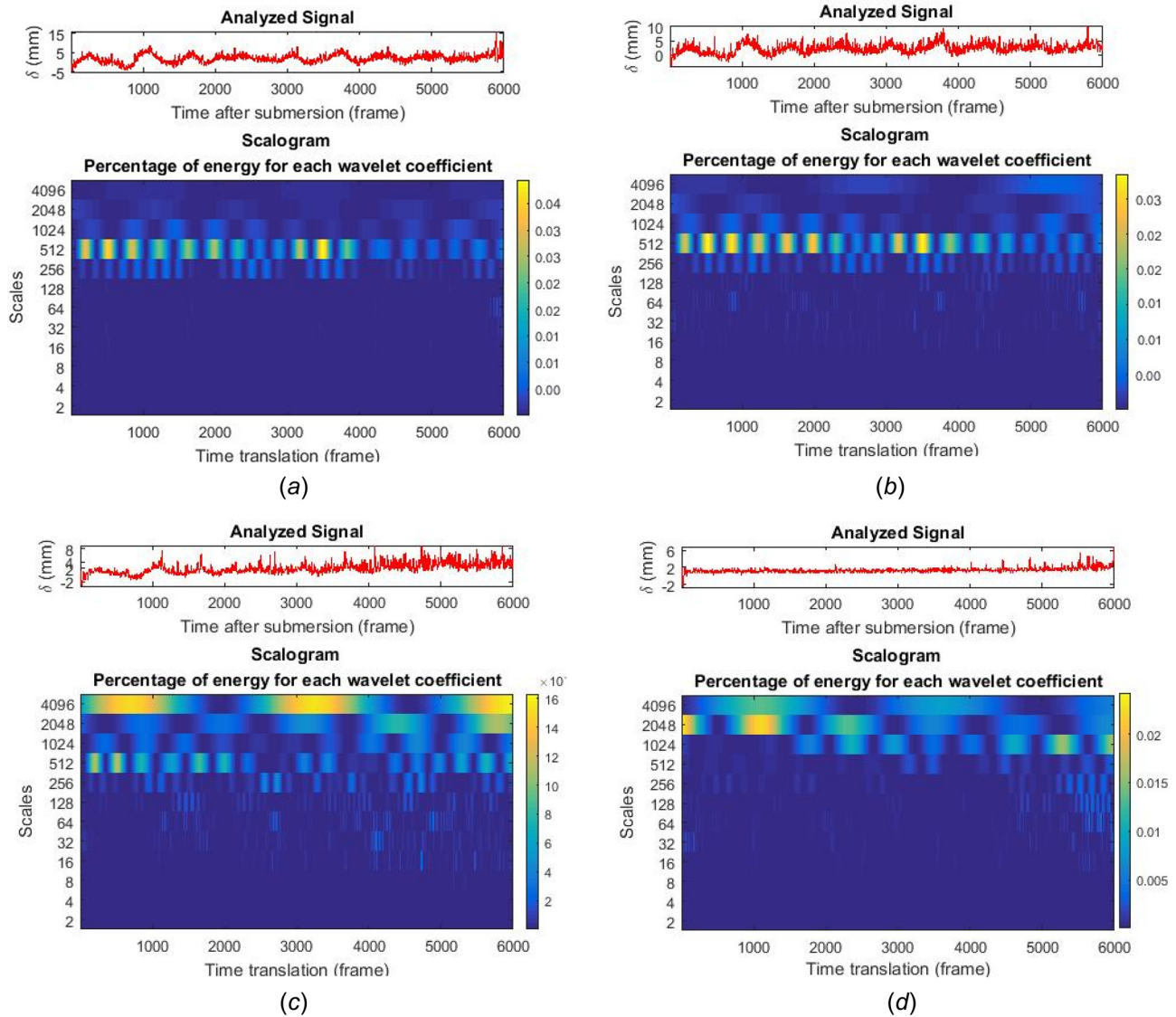


**Fig. 4** Multiresolution analysis of signals in the first 6000 frames. The Wavelet basis db45 has been used for MRA: (a)  $\phi = 42$  deg, (b)  $\phi = 28$  deg, (c)  $\phi = 14$  deg, and (d)  $\phi = 0$  deg.

$$x_{\text{off}} = x_{\text{off}} + l_{\text{Rod}} \sin(\beta f_{1A}) \quad (13)$$

$$y_{\text{off}} = y_{\text{off}} + l_{\text{Rod}}(1 - \cos(\beta f_{1A})) \quad (14)$$

and repeating the signal extraction process as described in Sec. 2.

- (3) Usage of MRA to decompose the latest collected two-phase signals, and selection of wavelet coefficients corresponding to the scales that have higher intensities than other scales to construct an updated IA signal  $f_{1A\text{Updated}}$ .
- (4) Updating  $\beta$  based on the updated IA signal as

$$\beta \leftarrow (\beta + \mu \max(f_{1A\text{Updated}})) \quad (15)$$

where  $\mu$  is the step size (set to 0.001).

- (5) Repeating step (2) until intensity of IA signal is minimized.

Once the dominant portion of the IA signal is identified and  $\beta$  is determined, the dynamical angle  $\alpha$  can be obtained via  $\alpha = \beta f_{1A}$ , and the offset coordinates  $x_{\text{off}}$  and  $y_{\text{off}}$  are dynamically updated with respect to the IA signal via Eqs. (13) and (14), respectively. After extracting the IA signal (see Sec. 2) with the new dynamic parameters, the resulting vapor film signals are significantly denoised. Then, the aforementioned process is repeated on the

resulting signal by using MRA for the first  $\sim 9.2$  s and by extracting the wavelet coefficients that contribute to the low-frequency vibration in the IA signal. Figure 5 provides a schematic representation of the recursive filtering process. In the first iteration, the wavelet coefficients are extracted from scales of 256 and 512, and it is found that maximum  $\alpha = -1.317$  deg.

The intensity of inherent artifact signals is lower after implementation of the first iteration; however, in MRA analysis, low-frequency signals are still more observable at larger values of  $\phi$ . Therefore, another iteration is performed to extract wavelet

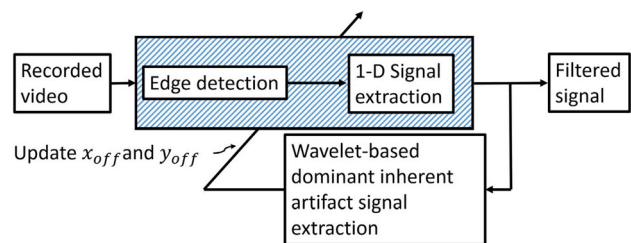


**Fig. 5** Schematic representation of the recursive filtering process

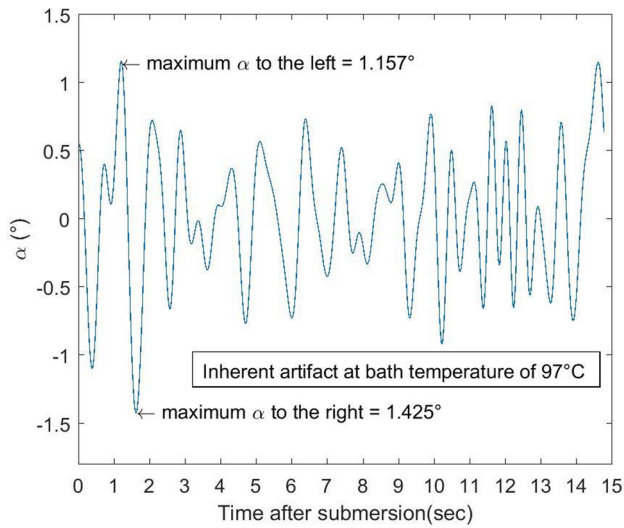


Fig. 6 Profile of a typical IA signal

coefficients from the 1024 scale to find the maximum value of  $\alpha \approx -0.252$  deg. The dominant IA signal is the sum of  $\alpha$  (in the first iteration) and  $\alpha$  (in the second iteration). Figure 6 shows the profile of a typical IA signal after executing two iterations of the recursive process. It is seen that the IA phenomenon can result in

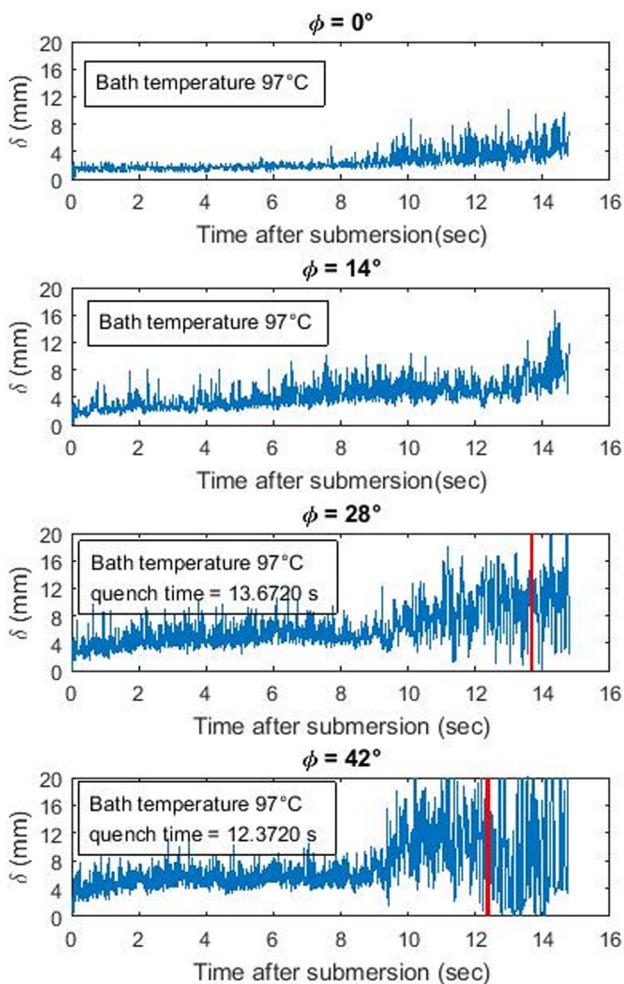


Fig. 7 Filtered signals of vapor film thickness. The thick vertical lines in the two bottom plots indicate the time of thermocouple quench.

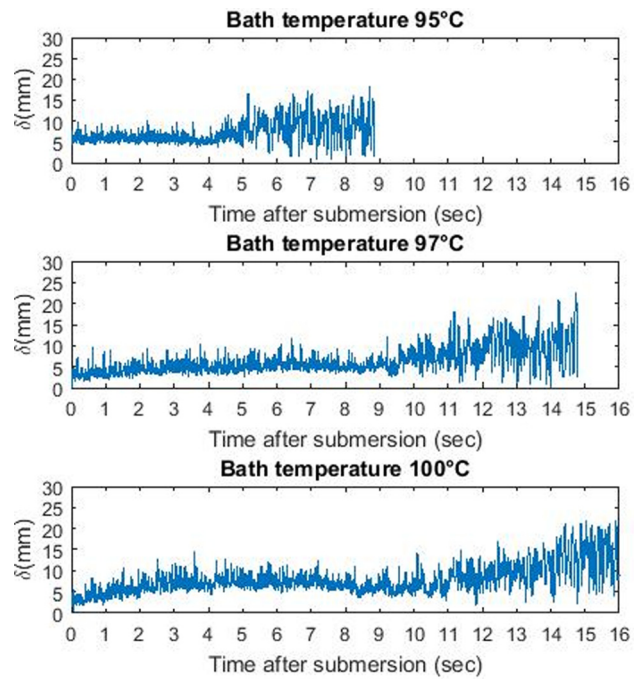


Fig. 8 Filtered signals ( $\phi = 28$  deg) at different bath temperatures

an pendulum motion with angles up to 1.157 deg to the left and 1.425 deg to the right.

Upon removal of the low frequency noise, the filtered signals are found to be in close agreement with the physics of the experiment and can be used to determine the accuracy of wavelet analysis for this application. Figure 7 compares the variations in temporal profiles of film thickness at different angular locations. It is seen that the vapor thickness becomes larger at higher angular locations due to the transition from film to nucleate boiling. The thick vertical lines in Fig. 7 indicate that, for angles  $\phi = 42$  deg and 28 deg, the respective thermocouples have been quenched (by water splashing) at  $\sim 12.37$  s and  $\sim 13.67$  s, respectively, from a higher angular location toward lower angular locations.

Figure 8 represents the profiles of film thickness  $\delta$  at  $\phi = 28$  deg for different liquid bath subcoolings. The value of this local  $\delta$  at 28 deg is found to decrease with increasing liquid subcooling temperatures. There are two heat transfer mechanisms at work when the liquid bath is subcooled. First, a part of the heat from the vessel wall is utilized to raise the liquid temperature, and the remaining heat is used for evaporation. Second, as the vapor film attempts to grow outward, it is condensed by the subcooled bulk liquid [11]. These are the two major reasons that lead to a lower film thickness with increased subcooling temperatures. Comparing the effects of angular location on film thickness for a 95 °C bath (i.e., 5 °C bath subcooling) in Fig. 8, it is seen that as the angular location increases, so does the film thickness. Here too, the inherent physics of the problem is used to confirm that the filtered signals are in agreement with the thermal-hydraulic phenomena in the experiment.

#### 4 Summary, Conclusions, and Future Work

This paper has presented the filtering of two-phase thermal-hydraulic signals by wavelet-based denoising. These signals are extracted from an experimental apparatus, where the two-dimensional images are first converted to a one-dimensional signal of vapor film thickness by making use of the geometrical properties and constraints of the problem. In these experiments, the recorded video images are contaminated by nonstationary low-frequency vibrations in the thermal-fluid environment, which are

deemed as the IA signals. These signals are identified recursively by using MRA with wavelet basis of db45, which reconstructs the wavelet coefficients which largely contribute to the IA vibration at scales of 256, 512, and 1024. In the recursive process, the IA vibration is found to contain a dynamic angle of oscillation, with a maximum value of 1.157 deg to the left and 1.425 deg to the right. With this dynamic angle as a critical parameter, the signal contamination can be removed during the film edge extraction process, and the filtered two-phase thermal-hydraulic signals are reproduced. Finally, the now filtered signals have been verified for their trends based on the inherent physics of the experiment.

While there are many theoretical and experimental applications of this new method for thermal-hydraulic signal filtering, the authors suggest the following topics to be addressed for future research:

- (1) Extension of the proposed method for stability analysis of two-phase thermal-hydraulic systems.
- (2) Robustness of the proposed method to unstructured (e.g., modeling) and structured (e.g., parametric) uncertainties and exogenous disturbances.
- (3) Applicability of the proposed method for online monitoring and control.

### Acknowledgment

Any opinions, findings, and conclusions or recommendations expressed in this publication are those of the authors and do not necessarily reflect the views of the sponsoring agencies.

### Funding Data

- U.S. Air Force Office of Scientific Research (AFOSR) under Grant No. FA9550-15-1-0400 in dynamic data-driven application systems (DDDAS).

### Nomenclature

$\hat{i}$  = horizontal direction  
 $\hat{j}$  = negative vertical direction

$l_{\text{Rod}}$  = length of the iron rod (Fig. 2(c))  
 $R$  = radius of the hemispherical vessel  
 $(x_{\text{im}}, y_{\text{im}})$  = the position of water surface at an angle  $\theta$   
 $x_{\text{off}}$  = horizontal distance: origin to vessel center  
 $y_{\text{off}}$  = vertical distance: origin to vessel center  
 $\alpha$  = dynamic angle due to IA vibration (Fig. 2(c))  
 $\beta$  = variable used for identification of  $\alpha$   
 $\delta$  = bubble thickness  
 $\theta$  = dummy variable for calculation of  $\phi$   
 $\phi$  = measurement angle  
 $(1, 1)$  = origin of the image in pixels

### References

- [1] Rouge, S., 1997, "Sultan Test Facility for Large-Scale Vessel Coolability in Natural Convection at Low Pressure," *Nucl. Eng. Des.*, **169**(1–3), pp. 185–195.
- [2] Chu, T., Bainbridge, B., Simpson, R., and Bentz, J., 1997, "Ex-Vessel Boiling Experiments: Laboratory- and Reactor-Scale Testing of the Flooded Cavity Concept for In-Vessel Core Retention—Part I: Observation of Quenching of Downward-Facing Surfaces," *Nucl. Eng. Des.*, **169**(1–3), pp. 77–88.
- [3] Brusstar, M., Merte, H., Keller, R., and Kirby, B., 1997, "Effects of Heater Surface Orientation on the Critical Heat Flux—I: An Experimental Evaluation of Models for Subcooled Pool Boiling," *Int. J. Heat Mass Transfer*, **40**(17), pp. 4007–4019.
- [4] Sohag, F., Beck, F., Mohanta, L., Cheung, F., Segall, A. E., Eden, T., and Potter, J., 2017, "Enhancement of Downward-Facing Saturated Boiling Heat Transfer by the Cold Spray Technique," *Nucl. Eng. Technol.*, **49**(1), pp. 113–122.
- [5] Sohag, F., Beck, F., Mohanta, L., Cheung, F., Segall, A., Eden, T., and Potter, J., 2017, "Effects of Subcooling on Downward Facing Boiling Heat Transfer With Micro-Porous Coating Formed by Cold Spray Technique," *Int. J. Heat Mass Transfer*, **106**, pp. 767–780.
- [6] Mallat, S., 2009, *A Wavelet Tour of Signal Processing*, 3rd ed., Academic Press, Amsterdam, The Netherlands.
- [7] De Kerpel, K., De Schampheleire, S., De Keulenaer, T., and De Paepe, M., 2015, "Two-Phase Flow Regime Assignment Based on Wavelet Features of a Capacitance Signal," *Int. J. Heat Fluid Flow*, **56**, pp. 317–323.
- [8] Nguen, V. T., Euh, D. J., and Song, C.-H., 2010, "An Application of the Wavelet Analysis Technique for the Objective Discrimination of Two-Phase Flow Patterns," *Int. J. Multiphase Flow*, **36**(9), pp. 755–768.
- [9] Marr, D., and Hildreth, E., 1980, "Theory of Edge Detection," *Proc. R. Soc. London B: Biol. Sci.*, **207**(1167), pp. 187–217.
- [10] Beck, F., Virani, N., Mohanta, L., Sohag, F., Ray, A., and Cheung, F., 2017, "An Image Processing Technique for the Study of Vapor Film Dynamics During Quenching of a Downward Facing Hemisphere," 16th International Topical Meeting on Nuclear Reactor Thermal Hydraulics (NURETH), Xian, China, Sept. 3–8.
- [11] Mohanta, L., Cheung, F., and Bajorek, S., 2016, "Stability of Coaxial Jets Confined in a Tube With Heat and Mass Transfer," *Physica A*, **443**, pp. 333–346.